



Fabrication and Characterization of Dye-Sensitized Solar Cells (DSSCs) using Flexible Non-conductive Polyetherimide (PEI) Polymer Substrate

H. P. Wante^{1*}, S. L. Yap², J. Aidan¹, A. Alkasim³

^{1*&2}Plasma Research Center, Department of Physics, University of Malaya, Kuala Lumpur, Malaysia

^{1*,1&3}Department of Physics Modibbo Adama University of Technology, Yola, Adamawa State, Nigeria.

Received 03 Sept 2020,
Revised 19 Oct 2020,
Accepted 21 Oct 2020

Keywords

- ✓ Photoelectrochemical
- ✓ DSSC
- ✓ Polyetherimide
- ✓ Efficiency
- ✓ Photocurrent

wante2h@gmail.com;
Phone: +234806455780;

Abstract

Efficient flexible dye-sensitized solar cells (DSSCs) using PEI polymer as supporting substrate for fabricating nanocrystalline TiO₂ film electrodes were developed, intending to improve the photoelectrochemical properties of plastic based-substrate DSSCs. The most important advantage of a flexible-based TiO₂ film electrode over a glass-based electrode lies in its flexibility, light weight and can be used for roll-roll mass production. In this paper, indium tin oxide (ITO) was coated at 50 nm, 100 nm and 200 nm for the fabrication of DSSCs using RF magnetron sputtering technique at lower temperature in order to make it conductive, but still transparent. The photocurrent of the flexible cell with a PEI/ITO-100nm/TiO₂ electrode produces an optimum solar conversion efficiency of 2.8% at 1000 mW/cm² light intensity and maximum power density of 2.69 mW/cm², based on short-circuit photocurrent density, open-circuit voltage and fill factor of 11.4 mA/cm², 0.63 V and 0.39, respectively.

1. Introduction

Dye-sensitized solar cell (DSSC) is a new type of thin film solar cell that converts light in a visible range into electricity by using photo-electrochemical system [1]. Solar energy is fast becoming the most viable, eco-friendly and sustainable alternative source of renewable energy [2]. For the fulfillment of increasing world energy consumption with less impact on the environment, photovoltaic (PV) technology is a suitable renewable power source [3]. In the last two decades, there has been a growing interest for the fabrication of low-cost and flexible solar cells. Presently, silicon based solar cells dominate the commercial market, but their manufacturing process is energy intensive under high vacuum conditions, leading to high manufacturing costs. In this regard, dye sensitized solar cells (DSSCs) have demonstrated their potentials as relatively low-cost alternatives to the silicon solar cells [4].

The DSSC captures sun rays to produce electrons, and it was conceived to mimic the photosynthetic process of chlorophyll [5]. For this reason, a nanostructured semiconductor is typically deposited onto a conductive substrate and, subsequently, sensitized with a molecular dye able to absorb in the visible range. The semiconductor-dye system is called photonode, and represents the core of the device [5]. Printing, blading and roll-to-roll technologies are important techniques proposed to fabricate standard DSSCs [6,7]. Recently, there has been an increased demand for light-weight and flexible electronic devices as they can be produced in large scales using printing techniques at room temperature with a

much-reduced production cost. It is well known that conventional DSSCs are usually fabricated on rigid transparent conducting oxide (TCO) glass substrates. This particular substrate, however, has some drawbacks with regards to its fragility, weight and rigidity, the later preventing roll-to-roll mass production and the integration of DSSCs in many portable devices [8]. By replacing this conventional glass substrate with a flexible polymer substrate, which is compatible with the continuous roll-to-roll process, would therefore result in far most cost-effective, flexible and lightweight solar cells. However, two major limitations with the plastic-based substrates are that they have lower efficiency compared to glass substrate DSSCs and their thermal instability at the high temperature (450-500 °C), which are required for sintering of TiO₂ photoelectrodes of DSSCs. However, some flexible substrates can only endure temperatures below 150 °C [9]. It must also be mentioned that these high temperatures of sintering increase the resistivity of the conducting substrate, particularly ITO [10]. These relatively high temperatures normally used in the annealing process of TiO₂ photoelectrodes production are only needed for two key reasons. The first one is to eliminate the organic surfactant present in the colloidal TiO₂ suspension or paste used to make the photoelectrodes. The second key reason is to improve the connection between the nanocrystallites that constitute the film (necking), as well as to guarantee their adherence to the transparent conducting oxide (TCO) film acting as substrate [10].

Electrolyte in DSSC is the medium for charge transportation between photoanode and counter electrode and acts as a source for dye regeneration [11]. The long-term stability of the device strongly depends on the electrolyte component. However, the highest efficiency reported in DSSC was by employing liquid electrolyte. But there are some impediments when using this liquid electrolyte like leakage while sealing, degradation of the polymer substrate and corrosion of the counter electrode etc., which prevent DSSC's from further application and commercialization [11]. So, as an alternative to liquid electrolyte, gel electrolytes were introduced. Thus, a gel electrolyte possesses both the cohesive property of solid as well as diffusive transport property of liquid [12].

Usually, indium tin oxide (ITO) coated polyethylene terephthalate (PET) or polyethylene naphthalate (PEN) are used as flexible base substrate for solar cells. A plastic substrate having higher thermal stability than that of PEN or PET substrate may result in more efficient solar cell [13]. Moreover, most of the flexible solar cells fabricated that use PET or PEN are already coated with ITO, but in this research, ITO was coated on PEI substrate using RF magnetron sputtering technique.

2. Materials and method

2.1 Materials

PEI substrate, TiO₂-P25 powder, ethanol, de-ionized water, iodide (gel electrolyte), platinum, ruthenium N3 dye, multimeter, ITO target, autoclave machine and RF magnetron sputtering machine.

2.2 Experimental method

The experimental method adopted in this research was that of [14]. Polyetherimide (PEI) has been adapted as a substrate for the fabrication of DSSCs because of its flexibility, transparency and high temperature resistance. Three labeled samples with dimensions of 20 mm × 20 mm and thickness of 0.2 mm were used in this work. ITO films were grown at different thicknesses using RF magnetron sputtering technique on the surface of PEI substrates in order to make the substrates conductive and still transparent. The sputtering system used utilizes a sintered ITO target having an In₂O₃:SnO₂ compositions of 90:10 wt.% with 99.99% purity was used as target (Table 1). The substrate temperature during deposition was maintained at low value. The resistivity of the ITO/PEI for different coating thicknesses was determined using standard four-point probe technique. The photoanode paste was deposited on the

conductive active area of the ITO/PEI using doctor blade technique [14]. Allowing it to dry at room temperature, the TiO₂ thin films were sintered at 200 °C in air to give nanocrystalline-TiO₂ films. After the annealing process of the photoanodes, the substrates were soaked in a dye solution for 24 h. In order to control the environment effect, the samples were stored in a closed space without the presence of light. Meanwhile, the counter electrode was fabricated by depositing platinum on the conductive surface of the ITO/PEI. Then, the complete DSSC structure was done by sandwiching the working electrode and counter electrode together using a binder spacer. Lastly, gel iodine solution was applied in between the two electrodes as a mediator for the redox process. The grain sizes (D) were determined from TiO₂ anatase XRD reflections using the Debye-Scherrer equation (1):

$$D = \frac{0.9\lambda}{\beta \cos \theta} \quad 1$$

where β is the peak width, θ is the diffraction angle and λ is the X-ray wavelength corresponding to Cu-K α radiation.

Table 1: Magnetron sputtering parameters

Parameters	Value
Distance of substrate to target	6.5 cm
Deposition pressure	8.6×10 ⁻⁴ Torr
Flow rate	50 sscm
Power	100 W
Speed	6 rpm

2.3 Synthesis of TiO₂ paste

Preparation of suitable TiO₂ pastes to produce high quality mechanically stable films without organic binders is one of the challenges when fabricating DSSCs on plastic substrates. In order to prevent film cracks due to large agglomerates, the TiO₂ nanoparticles are required to be well dispersed in the paste. TiO₂ paste was prepared by synthesizing TiO₂ powder with ethanol and de-ionized water for TiO₂ layer deposition without the use of any organic surfactant as binders. The mixture was stirred for 5 min for proper dilution of the compound and the TiO₂ powder, so that the TiO₂ particles were well dispersed in the paste. The paste prepared was deposited by doctor blade technique. After the deposition of TiO₂ layer, the samples were sintered at 200 °C in order to form nanocrystalline TiO₂ structure.

3. Results and discussion

ITO was initially deposited at 300 s on the substrate and after the deposition the thickness of the sample was determined using XRR (X-ray reflectivity) analysis which was found to be 88 nm at X-ray wavelength of 0.1540593 nm and step size of 0.005 as shown in the profile below. Figure 1 shows the XRR data measured for the ITO film deposited on the substrate at bias voltage of 0 V. Curve-fitting was performed by using the thickness, mass density and roughness of three layers composing the layered ITO structure as free parameters. In Figure 1, the amplitude of the oscillations gradually increased with increase in reflection angle. The modulation in the XRR of ITO film arises from interference between the X-ray scattered from the air and the PEI interface and hence the period of this oscillation is directly related to the thickness of the ITO film [15].

Figure 2 shows the profile for the thickness of the coating, which is the sum of the first three layers. The top layer which is also called a cap layer was ignored because its formation was as a result of roughness or oxidation or structure of the surface which has a lower density compared to other layers.

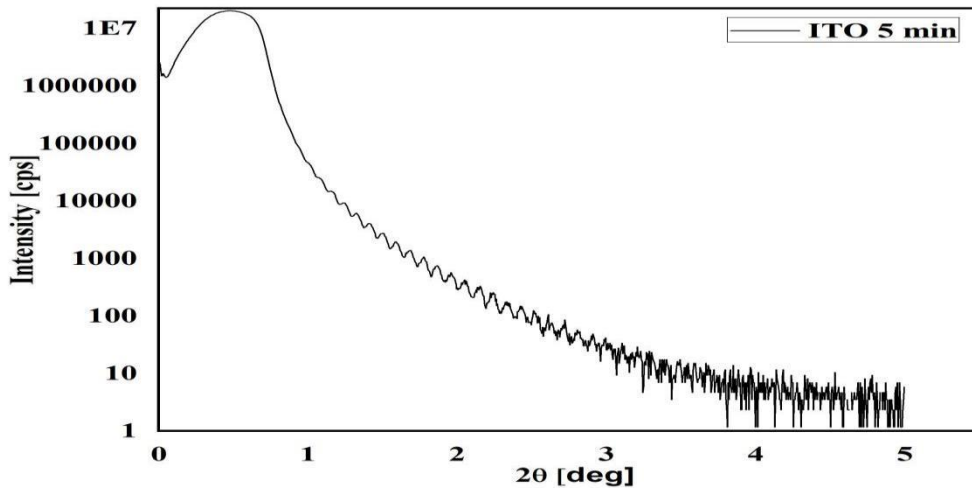


Figure 1: Variation of intensity with diffraction angle of XRR analysis of ITO deposited at 5 minutes.

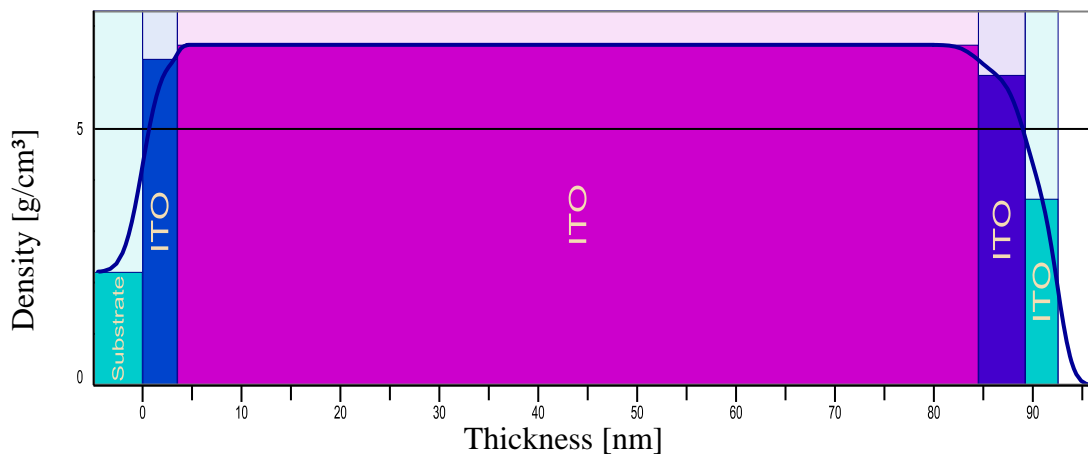


Figure 2: Profile of XRR analysis of ITO deposited for 5 mins

The thickness required were 50 nm, 100 nm and 200 nm, which were determined by adjusting the deposition time calculated from equation (2):

$$\frac{300s}{88nm} \times \tau = t \quad (2)$$

where τ is the desired thickness of the coating and t is the time taken for the sample to be coated. The band gaps (E_g) of 50 nm, 100 nm and 200 nm thicknesses were obtained by extrapolating the linear sections of the absorption curves towards the x-axis, as shown in Figures 3, 4 and 5.

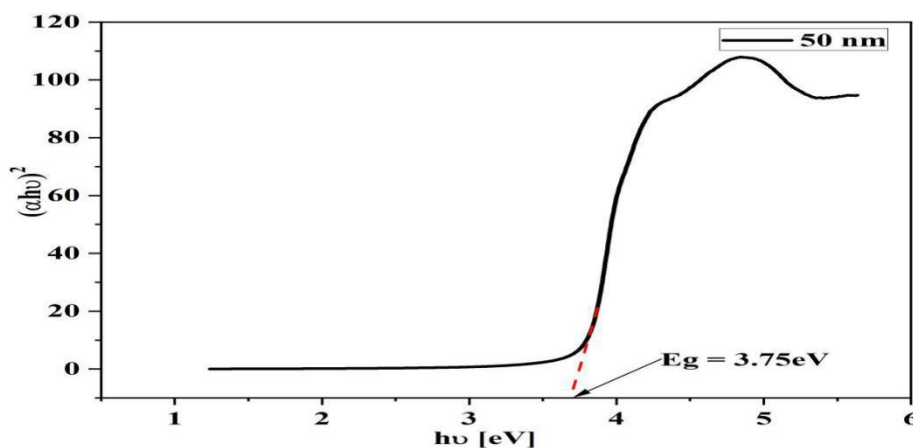


Figure 3: Variation of $(\alpha h\nu)^2$ at thickness of 50 nm with photon energy

The variations in the band gaps (from 3.75 eV to 3.57 eV) are associated with the film thicknesses and consequently with the interference in the ITO layer. In Figures 3, 4 and 5, it could be observed that the band gap energy decreases with increasing ITO thickness which agrees with the results of [16]. The reason for the variation is the result of increase in number of carriers, which leads to an increase in the Fermi level above the bottom of the conduction band, thereby causing enlargement in the optical band gap [17].

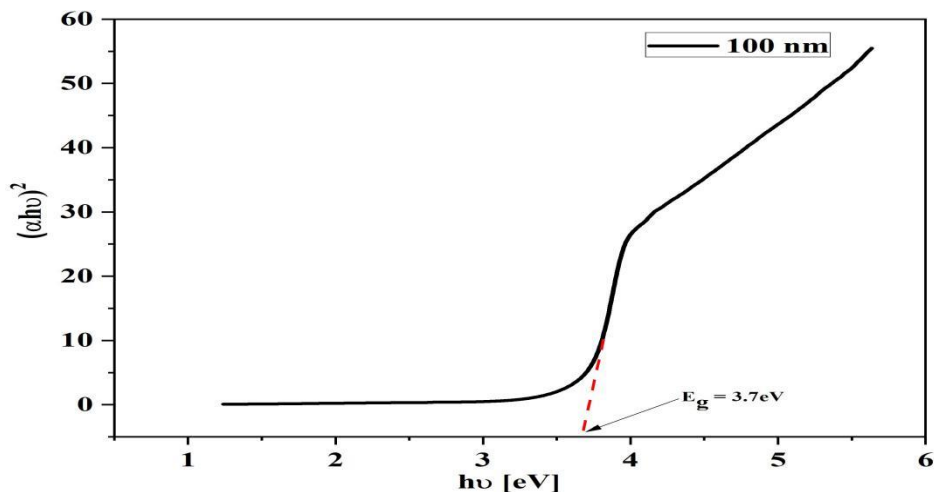


Figure 4: Variation of $(\alpha hv)^2$ at thickness of 100 nm with photon energy

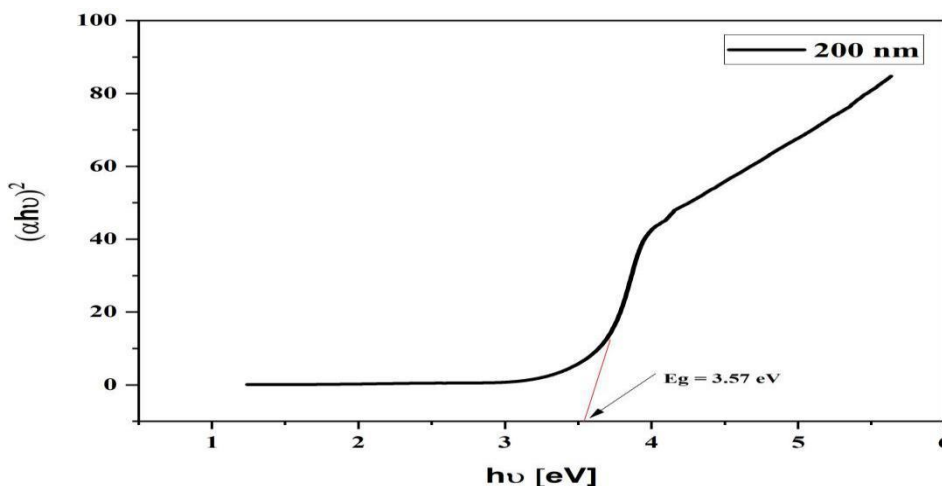


Figure 5: Variation of $(\alpha hv)^2$ at thickness of 200 nm with photon energy

3.1 Electrical characteristics

Surface electrical resistivity of the ITO films annealed at different thicknesses was measured using four-point probe technique. From Table 2, it is obvious that the resistivity reveals strong dependence on the substrate thickness.

Table 2: Electrical characteristics

Sheet resistivity, R_{sh} (Ω)	Thickness, t (nm)	Resistivity ρ ($\mu\Omega m$)	Conductivity (Ωm) ⁻¹
1.91E+02	50	9.54188	104801.2
7.54E+01	100	7.54344	132565.5
2.53E+01	200	5.05721	197737.5

The variation in electrical resistivity of the ITO films is from 9.54188×10^{-06} to 5.05721×10^{-06} . It is clear that the electrical resistivity of the ITO films dramatically decreases with increasing thickness. This is because of the fact that, to get more uniform ITO film, thickness should increase to have less impact of

the roughness due to the substrate. One can conclude that the lower resistivity ($5.05721 \times 10^{-06} \Omega\text{m}$) at thickness of (200 nm) is a result of an improved crystallinity, high oxygen vacancy concentration and grain growth, which reduces grain boundary scattering and surface roughness [18].

3.2 Fabrication of photoanode

TiO₂ paste was first prepared with organic surfactant (polyethylene glycol) without adding ethanol; however, the TiO₂ film prepared had very weak adhesion properties at low temperature sintering and peeled off easily from the conducting PEI polymer after heating. Therefore, the data for the zero ratio of ethanol/TiO₂ is not presented in this study. TiO₂ paste was later prepared using ethanol and small amount of de-ionized water because ethanol has a very low surface tension.

After the first photoanode was fabricated, the commercial liquid electrolyte was applied to the photoanode before sandwiching with the counter electrode; the flexible photoanode was deformed instantly after the application of the liquid electrolyte. This means that the commercial liquid electrolyte is not suitable for flexible polymer materials or it could be as results of much concentration of the electrolyte. Finally, gel electrolyte was used in place of commercial liquid electrolyte.

Figure 6 shows the experimental XRD pattern of TiO₂ nanoparticles at 10 μm thickness. Strong diffraction peak at 26.33° could be seen and the fitted peak gives the full width of half maximum (FWHM) 1.42° and area of 76593.57. From this study, considering the peak in degrees, average particle size of 5.72 nm and d-spacing of 3.39 Å for TiO₂ at 10 μm have been obtained by using Debye-Scherrer formula, equation 1. The experimental XRD pattern of TiO₂ agrees with that of [19,20].

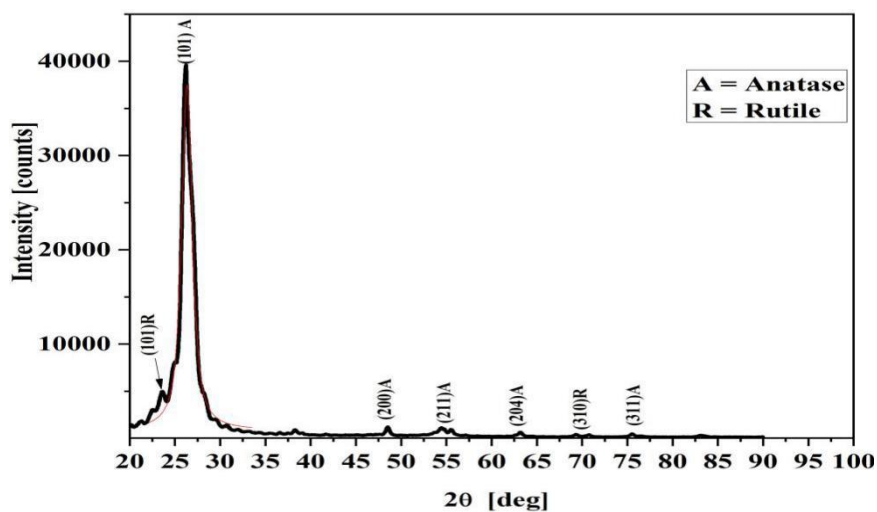


Figure 6: XRD pattern of TiO₂ nanoparticles with 10 μm thickness

Figures 7 and 8 showed the surface morphology observed for TiO₂ photoanode prepared by doctor blade at annealing temperature of 200 °C. Observed in surface morphology of TiO₂ photoanode is the spherical agglomeration of the nanostructure which is in accordance with that of [21].

Figure 8 presents the cross-sectional view of FE-SEM image of TiO₂ P25 based film prepared using doctor blade method at an annealing temperature of 200 °C. No visible changes in the morphology of the TiO₂ surface is expected in all the samples [22], since the TiO₂ paste was prepared under the same condition and deposited using the same method. The cross-sectional view shows clearly the evidence of a second phase interfacial layer between TiO₂ and ITO layer. The FE-SEM images also reveal that the TiO₂ film is uniform and crack-free on the surface. In addition, TiO₂-P25 layer exhibits a nanocrystalline and nanoporous structure which is composed of inter-connected nanoparticles as also proven by XRD analysis.

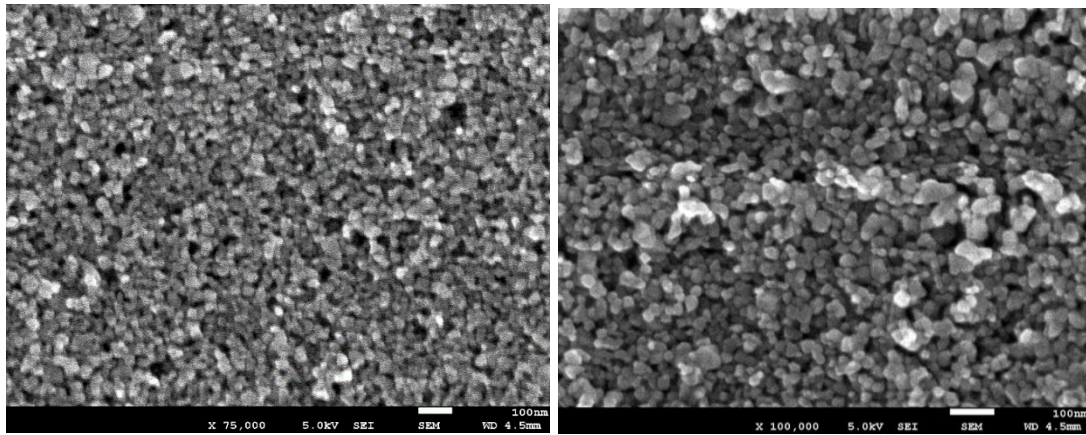


Figure 7: FESEM images of coated TiO₂ at higher magnification.

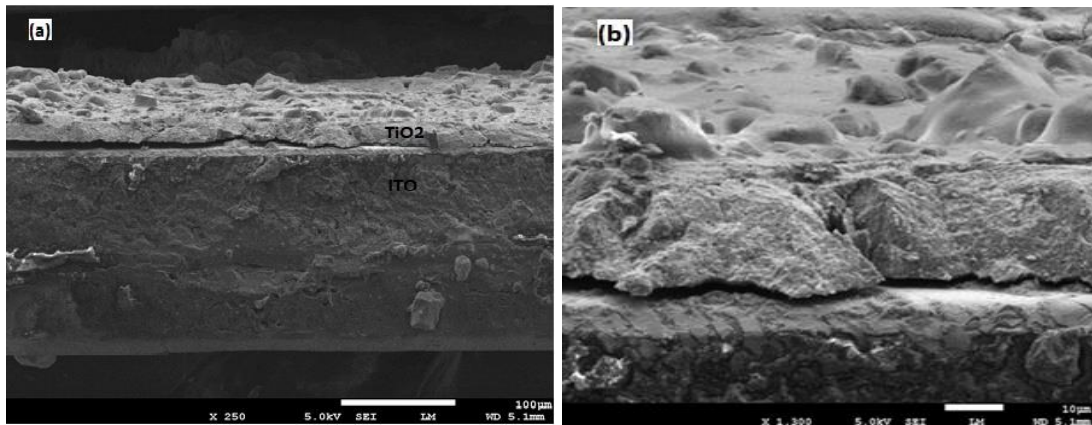


Figure 8: Cross-sectional view of FESEM images of TiO₂ coated on ITO (a) at 250 magnification and 100 μm scale and (b) at 1300 magnification and 10 μm scale.

3.3 J-V characteristics

J–V characteristics and power density curves of DSSCs using Pt counter electrodes for ITO coating of 50 nm, 100 nm and 200 nm with 10 μm thickness of TiO₂ are presented in Figures 9, 10 and 11, respectively.

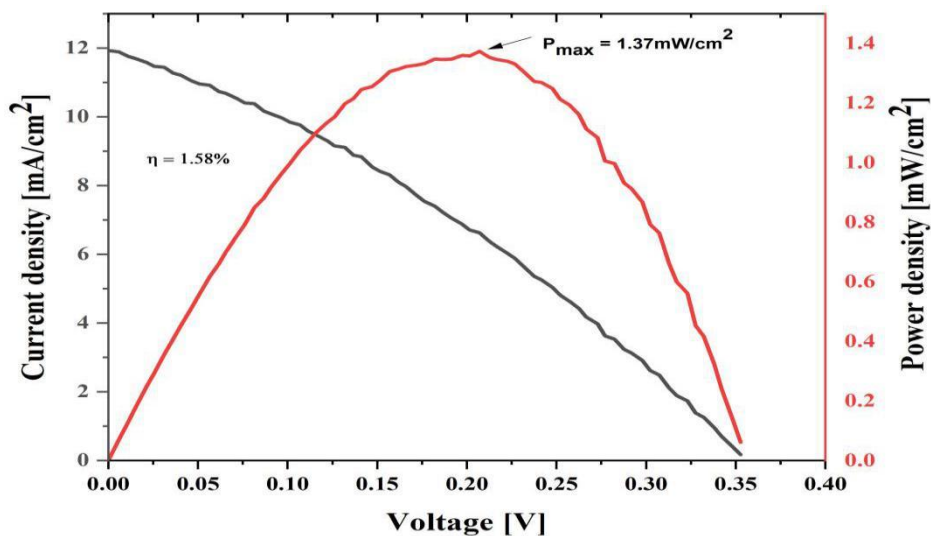


Figure 9: J-V and power density curves for 50 nm ITO coating at 10 μm thickness of TiO₂ and power density variation with voltage for 50 nm TiO₂.

The differences between J-V plots of the fabricated DSSCs in Figures 9, 10 and 11 are related to the amount of N3 dye bound to TiO₂ surface and the thickness of the TiO₂ film deposited [23]. The optimal efficiency achieved was 2.8 % which is agreement to that of [24] and maximum power density was 2.69 mW/cm² for ITO-100nm. This result showed that the 100 nm layers deposited on PEI flexible substrate was the optimal thickness to improve dye loading and to reduce the charge recombination rate [25].

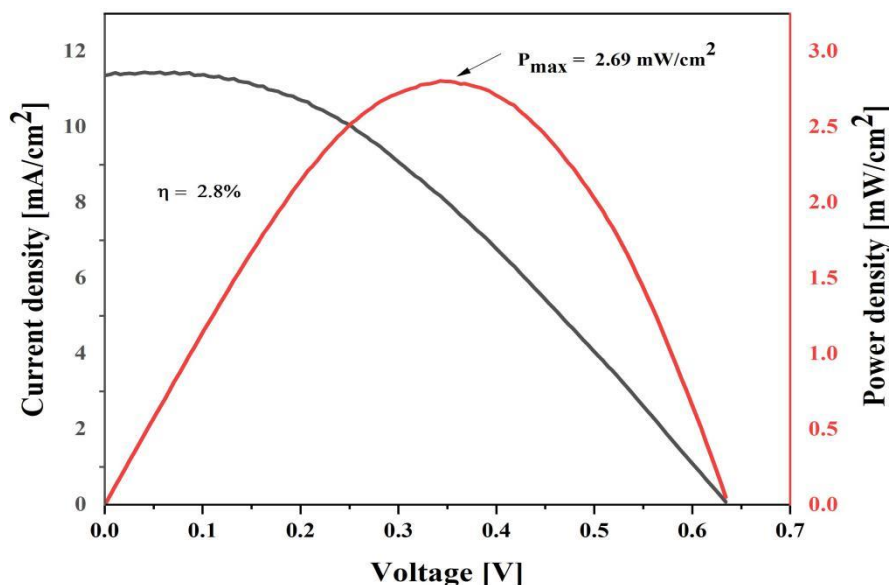


Figure 10: J-V and power density curves for 100 nm ITO coating at 10 μm thickness of TiO₂ and power density variation with voltage for 100 nm TiO₂.

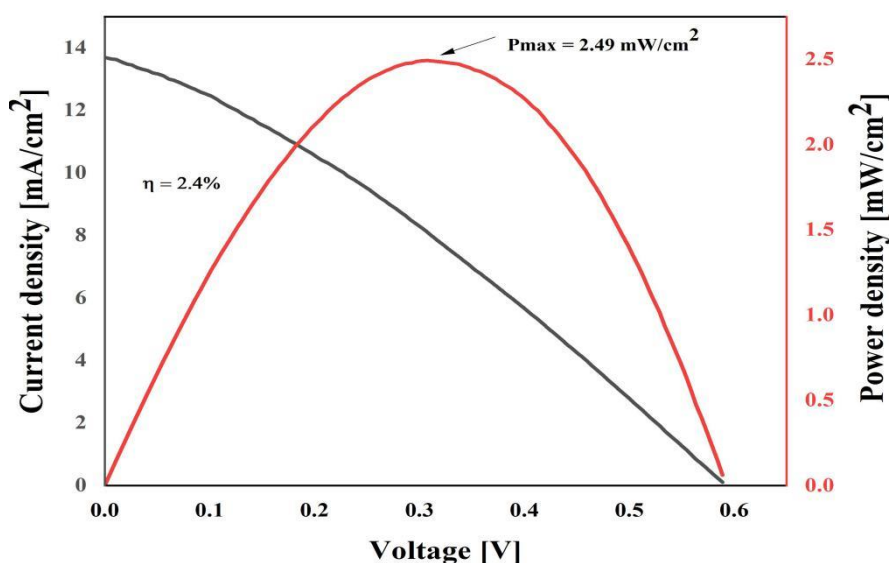


Figure 11: J-V and power density curves for 200 nm ITO coating at 10 μm thickness of TiO₂ and power density variation with voltage for 200 nm TiO₂.

Table 3: Properties of DSSCs.

Cell ID	J _{sc} [mA/cm ²]	V _{oc} [V]	FF	η [%]	P _{max} [mW/cm ²]
ITO (50nm)/TiO ₂	11.93	0.35	0.36	1.58	1.37
ITO (100nm)/TiO ₂	11.4	0.63	0.39	2.8	2.69
ITO (200nm)/TiO ₂	13.7	0.59	0.3	2.4	2.49

Conclusion

In conclusion, fabrication and characterization of DSSCs using flexible PEI substrate was achieved. ITO films were grown at different thicknesses using RF magnetron sputtering technique on the surface of PEI substrates in order to make the substrates conductive and still transparent. TiO₂ paste was prepared without the use of any organic surfactant as binder. Three labelled samples were prepared as photoanode and the optimal efficiency achieved was 2.8% and maximum power density was 2.69 mW/cm² for ITO-100 nm. We concluded that the 100 nm layers deposited on PEI flexible substrate was the optimal thickness to improve dye loading and to reduce the charge recombination rate of flexible DSSCs.

References

1. A. N. B. Zulkifili, T. Kento, M. Daiki, & A. Fujiki. The basic research on the dye-sensitized solar cells (DSSC). *Journal of Clean Energy Technologies*, 3(5) (2015) 382-387.
2. W. Ghann, H. Kang, T. Sheikh, S. Yadav, T. Chavez-Gil, F. Nesbitt, J. Uddin. Fabrication, optimization and characterization of natural dye sensitized solar cell. *Scientific Reports*, 7(1) (2017) 1-12.
3. A. Goetzberger, & C. Hebling. Photovoltaic materials, past, present, future. *Solar Energy Materials and Solar Cells*, 62(1-2) (2000) 1-19.
4. H. C. Weerasinghe, F. Huang & Y. B. Cheng. Fabrication of flexible dye sensitized solar cells on plastic substrates. *Nano Energy*, 2(2) (2013) 174-189.
5. F. Bella, A. Verna & C. Gerbaldi. Patterning dye-sensitized solar cell photoanodes through a polymeric approach: A perspective. *Materials Science in Semiconductor Processing*, 73 (2018) 92-98.
6. F. Bella, S. Galliano, G. Piana, G. Giacona, G. Viscardi, M. Gratzel, C. Barolo & C. Gerbaldi. Boosting the efficiency of aqueous solar cells: A photoelectrochemical estimation on the effectiveness of TiCl₄ treatment. *Electrochimica Acta*, 302 (2019) 31-37.
7. F. Bella, L. Porcarelli, D. Mentione, C. Gerbaldi, C. Barolo, M. Gratzel & D. Mecerreyes. A water-based and metal-free dye solar cell exceeding 7% efficiency using a cationic poly(3,4-ethylenedioxythiophene). *Chem. Sci.*, 11 (2020) 1485.
8. K. Yoo, Y. Y. Kim, J. A. Lee, J. S. Kim, D. K. Lee, K. Kim, J. Y. Kim, B. Kim, H. Kim & W. m. Kim. Completely transparent conducting oxide-free and flexible dye-sensitized solar cells fabricated on plastic substrates. *ACS nano*, 9(4) (2015) 3760-3771.
9. L. Zhang & A. Konno. Development of flexible dye-sensitized solar cell based on pre-dyed zinc oxide nanoparticle. *Int. J. Electrochem. Sci*, 13 (2018) 344-352.
10. D. Gutiérrez-Tauste, I. Zumeta, E. Vigil, M. A. Hernández-Fenollosa, X. Domènech & J. A. Ayllón. New low-temperature preparation method of the TiO₂ porous photoelectrode for dye-sensitized solar cells using UV irradiation. *Journal of Photochemistry and Photobiology A: Chemistry*, 175(2-3), (2005) 165-171.
11. P. Nijisha, N. M. Bhabhina, S. Sindhu. Application of gel electrolyte in dye sensitized solar cells. *Nanosystems: Physics, Chemistry and Mathematics*, 7(4) (2016) 752-754.
12. W. Kubo, K. Murakoshi, T. Kitamura, S. Yoshida, M. Haruki, K. Hanabusa, H. Shirai, Y. Wada & S. Yanagida. Quasi-solid-state dye-sensitized TiO₂ solar cells: Effective charge transport in mesoporous space filled with gel electrolytes containing iodide and iodine. *J. Phys. Chem. B*, 1059 (2001) 12809-12815.

13. H. P. Wante, S. L. Yap, J. Aidan & P. Saikia. Efficiency Enhancement of Dye Sensitized Solar cells (DSSCs) by Atmospheric DBD Plasma Modification of Polyetherimide (PEI) Polymer Substrate, *J. Mater. Environ. Sci.*, 11(5) (2020) 713-722.
14. L. Chen, W. Tan, J. Zhang, X. Zhou, X. Zhang & Y. Lin. Fabrication of high performance Pt counter electrodes on conductive plastic substrate for flexible dye-sensitized solar cells. *Electrochimica Acta*, 55(11) (2010) 3721-3726.
15. C. Park, S. Chang, H. Uhm, S. Seo & J Park. XPS and XRR studies on microstructures and interfaces of DLC films deposited by FCVA method. *Thin Solid Films*, 420 (2002) 235-240.
16. S. Mohamed, F. El-Hossary, G. Gamal & M. Kahlid. Properties of indium tin oxide thin films deposited on polymer substrates. *Acta physica polonica A*, 115(3) (2009) 704-708.
17. L. Dong, G. Zhu, H. Xu, X. Jiang, X. Zhang, Y. Zhao, D. Yan, L. Yuan & A. Yu. Fabrication of Nanopillar Crystalline ITO Thin Films with High Transmittance and IR Reflectance by RF Magnetron Sputtering. *Materials*, 12(6) (2019) 958.
18. M. Ali, K. Ibrahim, O. S. Hamad, M. Eisa, M. Faraj & F. Azhari. Deposited indium tin oxide (ITO) thin films by dc-magnetron sputtering on polyethylene terephthalate substrate (PET). *Romanian Journal of Physics*, 56(5-6) (2011) 730-741.
19. R. Sonawane, B. Kale & M. Dongare. Preparation and photo-catalytic activity of Fe \square TiO $_2$ thin films prepared by sol-gel dip coating. *Materials Chemistry and Physics*, 85(1) (2004) 52-57.
20. S. Takeda, S. Suzuki, H. Odaka & H. Hosono. Photocatalytic TiO $_2$ thin film deposited onto glass by DC magnetron sputtering. *Thin Solid Films*, 392(2) (2001) 338-344.
21. N. Jamalullail, I. Smohamad, M. Nnorizan & N. Mahmed. *Enhancement of energy conversion efficiency for dye sensitized solar cell using zinc oxide photoanode*. Paper presented at the IOP Conf. Ser. Mater. Sci. Eng. (2018).
22. S. Sheehan, P. Surolia, O. Byrne, S. Garner, P. Cimo, X. Li, D. Dowling & K. Thampi. Flexible glass substrate-based dye sensitized solar cells. *Solar energy materials and solar cells*, 132 (2015) 237-244.
23. S. A. Mozaffari, M. Saeidi & R. Rahmanian. Photoelectric characterization of fabricated dye-sensitized solar cell using dye extracted from red Siahkooti fruit as natural sensitizer. *Spectrochimica Acta Part A: Molecular and Biomolecular Spectroscopy*, 142 (2015) 226-231.
24. L. Y. Lin, C. P. Lee, K. W. Tsai, M. H. Yeh, C. Y. Chen, R. Vittal, C. G. Wu & C. K. Ho, Low-temperature flexible Ti/TiO $_2$ photoanode for dye-sensitized solar cells with binder-free TiO $_2$ paste. *Progress in Photovoltaics: Research and Applications*, 20(2), (2012) 181-190.
25. M.Q. Lokman, S. Shafie, S. Shaban, F. Ahmad, H. Jaafar, R. Mohd Rosnan, H. Yahaya, S.S Abdullah, Enhancing photocurrent performance based on photoanode thickness and surface plasmon resonance Using Ag-TiO $_2$ Nanocomposites in Dye-Sensitized Solar Cells. *Materials*, 12(13) (2019) 2111.

(2020) ; <http://www.jmaterenvironsci.com>